New Multifunctional Benzophenone-based Photoinitiators with High Migration Stability and the Application in 3D Printing

Shaohui Liu, Bernadette Graff, Damien Brunel, Guillaume Noirbent, Alexandre Mau, Hong Chen, Fabrice Morlet-Savary, Didier Gigmes, Pu Xiao, Frédéric Dumur, et al.

New Multifunctional Benzophenone-based Photoinitiators with High Migration Stability and the Application in 3D Printing

Shaohui Liu[1,2], Damien Brunel[3], Guillaume Noirbent[3], Alexandre Mau[1,2], Hong Chen[1,2], Fabrice Morlet-Savary[1,2], Didier Gigmes[3], Pu Xiao[4]*, Frédéric Dumur[3]*, Jacques Lalevée[1,2]*

[1]Université de Haute-Alsace, CNRS, IS2M UMR 7361, F-68100 Mulhouse, France
[2]Université de Strasbourg, France
[3]Aix Marseille Univ, CNRS, ICR UMR 7273, F-13397 Marseille, France
[4]Research School of Chemistry, Australian National University, Canberra, ACT 2601, Australia
*Corresponding authors: pu.xiao@anu.edu.au; Frederic.dumur@univ-amu.fr; jacques.lalevee@uha.fr

Abstract: In this paper, seven new photoinitiators based on the benzophenone scaffold are specifically designed for photopolymerization under mild conditions upon light-emitting diodes (LEDs) irradiation i.e. four benzophenone-triphenylamine photoinitiators (noted BT1-BT4) and three benzophenone-carbazole photoinitiators (noted BC1-BC3). Noticeably, these structures have never been reported in the literature except BT4 so that these molecules have been specifically designed for photopolymerization applications. Remarkably, various combinations of chemical groups were investigated in this work to determine the effects of the substitution pattern on their photoinitiation abilities. The formation of benzophenone-triphenylamine and benzophenone-carbazole hybrid structures not only contributes to red-shift the absorption maxima but also strongly enhances their molar extinction coefficients. The different compounds showed high photoinitiation abilities upon irradiation with a LED@405 nm, and the free radical photopolymerization of acrylates and the cationic polymerization of epoxides could be promoted with high final function conversions (e.g. 77% for BT3/iodonium salt/amine system in free radical photopolymerization). Markedly, because of the benzophenone moiety, a monocomponent Type II PI behavior

could be observed e.g. these compounds could initiate the polymerization alone. Remarkably, benzophenone-triphenylamine compounds BT2, BT3 and BT4 exhibited better hydrogen abstraction abilities as Type II photoinitiators than the benchmark and commercial photoinitiator 2-isopropylthioxanthone in the absence of amines as well as in the presence of amines. Furthermore, the interaction between the photoinitiators and the different additives were investigated by the steady state photolysis and fluorescence quenching experiments. The free radical generation in the BT3/amine system was confirmed by electron spin resonance-spin trapping technique, and the chemical mechanisms related to the polymerization efficiency are discussed. In addition, the migration stability of BT3 was investigated which was excellent due to its high molecular weight and its trifunctional character. Finally, the three-component photoinitiating system based on BT3 was successfully applied in 3D printing and the 3D patterns showed a remarkable spatial resolution.

Keywords: benzophenone, carbazole, photoinitiator, 3D printing, low migration

1. Introduction

Photopolymerization or light-induced polymerization has greatly progressed during the last decade with the development of new photoinitiating systems activable under low light intensity and under visible light. Compared to the thermal polymerization, photopolymerization exhibits many advantages including less energy consumption, excellent spatial and temporal control, no emission of volatile organic compounds and so on[1-4]. Besides coatings, adhesives and other conventional industries, photopolymerization has already found applications in many cutting-edge areas, including biomaterials and 4D printing[5-7]. For the moment, a large portion of the benchmark photoinitiators (PIs) are only adapted for UV irradiation and cannot even be activated in the near UV and the visible regions, such as benzoin for Type I cleavage PI and benzophenone for Type II H-abstraction PI. However, near UV and visible regions are now widely employed for the scientific research and industrial production[8,9]. Meanwhile, there are some obvious drawbacks for UV light source including harmful,

expensive, heat release that block the development of photopolymerization[10]. Nowadays, light-emitting diodes (LEDs) as irradiation sources become more widespread due to long emission wavelengths, good security and low cost[11]. In recent years, LEDs have shown a tremendous potential as an alternative to the traditional UV irradiation sources[12-13]. Therefore, it is important to develop new photoinitiating systems (PISs) which could match the emission spectra of LEDs in the near UV and the visible regions[4,14,15].

Dye-photosensitized systems are able to initiate free radical photopolymerizations (FRP) and cationic photopolymerizations (CP) and display a lively interest under LEDs irradiation[16,17]. In the excited state, organic dyes can interact with additives to generate active species capable to induce the polymerization of monomers and oligomers. A variety of organic dyes with wide absorption bands in near UV and visible regions have been found and numerous PISs based on organic dyes have been reported[16]. Carbazole, triphenylamine, pyrene, chalcone, etc. derivatives have been designed through chemical engineering and showed good performances in FRP and CP[18-25].

In this research, novel benzophenone-based PIs are proposed; interestingly, all the structures examined in this work have never been synthesized and even reported except BT4 that was designed as hole-transport materials for organic light-emitting diodes (see Scheme 1). Because of the benzophenone moiety in the structures, these PIs can be considered as promising Type II PIs in the presence of amines (electron donor) for the FRP. Triphenylamine and carbazole moiety acting as the photosensitizers can interact efficiently with an iodonium salt (electron acceptor) in both FRP and CP. Through the combination of benzophenone and triphenylamine (or carbazole) scaffolds in these PI structures, red-shifted light absorption maxima and high extinction coefficients could be achieved. Moreover, excellent photoinitiation performances were obtained in the presence of two or three-component systems, outperforming the benchmark benzophenone and 2-isopropylthioxanthone (ITX)-based Type II systems. The migration stability of the novel PIs and their applications in 3D printing were also investigated.

Commenté [FD1]: Pleas add this reference in the list. Y. Liu, X. Chen, Y. Lv, S.W.Y. Chen, J. Lam, F. Mahtab, H.S. Kwok, X. Tao, B.Z. Tang, Systemic Studies of Tetraphenylethene–Triphenylamine Oligomers and a Polymer: Achieving Both Efficient Solid-State Emissions and Hole-Transporting Capability. Chemistry – A European Journal 2012, 18, 9929–9938

2. Experimental section

2.1. Materials

Chemical structures of PIs are presented in the Scheme 1. Bis(4-*tert*-butylphenyl)iodonium hexafluorophosphate (Iod), ethyl 4-(dimethylamino)benzoate (EDB), benzophenone (BP) and 2-isopropylthioxanthone (ITX) were obtained from Lambson Ltd (Wetherby, United Kingdom). Phenyl-*N*-*tert*-butylnitrone (PBN) used as free radical trapping agent was purchased from TCI-Europe (Paris, France). Trimethylolpropane triacrylate (TMPTA) and (3,4-epoxycyclohexane)methyl 3,4-epoxycyclohexylcarboxylate (EPOX) were obtained from Allnex (Ivry sur Seine, France) and used as monomers for the free radical photopolymerization and the cationic photopolymerization respectively. The structures of some compounds used in this study are given in Scheme 2.

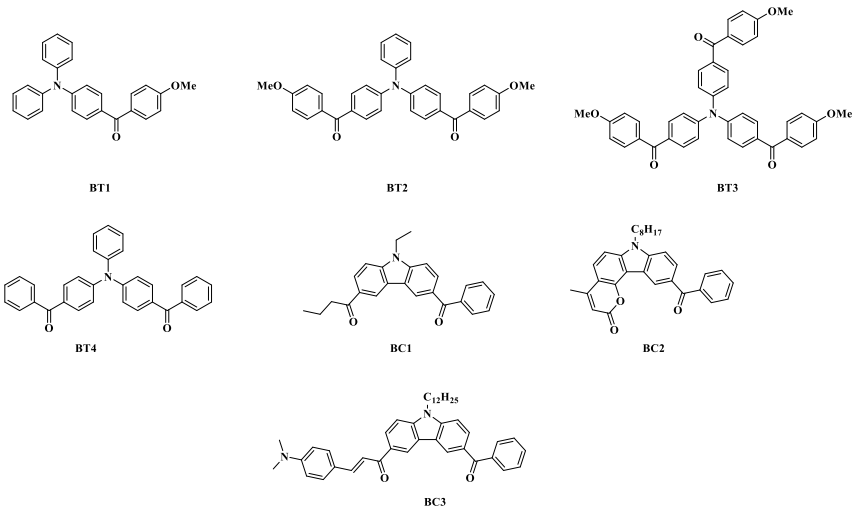

Scheme 1. The structures of PIs studied in this study.

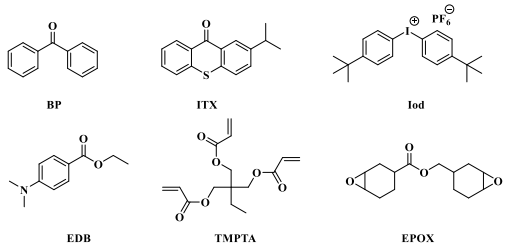

Scheme 2. The structures of other chemicals used in this study.

2.2. UV-visible absorption spectra

UV–visible absorption properties of the different PIs were investigated in acetonitrile using JASCO V730 spectrometer (JASCO, Lisses, France). Steady state photolysis studies of the PISs were studied under LED@405 nm irradiation, and the concentration of PIs was 5×10^{-5} M, the concentration of iodonium salt (Iod) and amine (EDB) was 0.01 M.

2.3. Free radical photopolymerization and cationic photopolymerization

The different components used in the PISs were added into a glass bottle and stirred overnight in the dark. The molar fraction of PIs and co-initiators were calculated from the monomer content (e.g. PI/Iod (0.5%/1% mol/mol) = PI: 0.005 mol, Iod: 0.01 mol, monomer: 1 mol). The FRP of TMPTA was carried out in laminate with a thickness of about 25 μm (between two polypropylene films to reduce the O_2 inhibition). For the CP of EPOX, the photosensitive resins (thickness ~ 25 μm) were irradiation under air. The conversion of acrylate functions of TMPTA and epoxy groups of EPOX were continuously evaluated by the Real-Time Fourier Transformed Infrared Spectroscopy JASCO FTIR 4700 (JASCO, Lisses, France) at about 1630 cm^{-1} and 790 cm^{-1} respectively. The irradiation starts from t = 10 s. A LED@405 nm was used as the irradiation source for photopolymerization and the light intensity at sample surface was about 110 $mW\cdot cm^{-2}$.

2.4. Fluorescence experiments

Fluorescence spectra of the different compounds were studied using the JASCO FP-6200 spectrometer (Jasco, Lisses, France). The concentration of PIs was 5×10^{-5} M in acetonitrile for fluorescence quenching experiments. The fluorescence lifetimes were determined by time-resolved fluorescence spectrometer (Jobin-Yvon Fluoromax 4). The interaction rate constants k_q between the PIs and additives (Iod and EDB) were extracted from classical Stern–Volmer equation ($I_0/I = 1 + k_q\tau_0$[additive]; where I_0 and I stand for the fluorescence intensity of the PIs in the absence and the presence of the additives respectively; τ_0 is the fluorescence lifetime of PIs in the absence of additives). The electron transfer quantum yields in the excited singlet state (Φ^{et}) were calculated from the equation $\Phi^{et} = k_q\tau_0$[additive]/(1+$k_q\tau_0$[additive]).

2.5. Redox potentials and free energy change

The redox potentials of the PIs (E_{ox} and E_{red}) were measured in acetonitrile by cyclic voltammetry using VoltaLab PST006 and tetrabutylammonium hexafluorophosphate as the supporting electrolyte (potentials vs. Saturated Calomel Electrode – SCE). Furthermore, the free energy change ΔG for the interaction of the PIs with additives for the electron transfer reactions in the excited state were calculated from the equation $\Delta G = E_{ox} - E_{red} - E^* + C$ (Where E_{ox}, E_{red} and E^* are the oxidation potential of the electron donor, the reduction potential of the electron acceptor and the excited state energy level respectively; C is neglected as usually done for polar solvents). Oxidation potential of EDB is 1.0 V and reduction potential of Iod is -0.7V[1,26].

2.6. Electron spin resonance - spin trapping (ESR-ST)

ESR-ST experiments were carried out using an X-band spectrometer (Bruker EMX-Plus). Phenyl-*N*-*tert*-butylnitrone (PBN) was selected as the free radical trapping agent. N_2 saturated *tert*-butylbenzene solutions were irradiated with a LED@405 nm in room temperature. Furthermore, the ESR spectra simulations were carried out with the PEST WINSIM program.

2.7 Migration study

0.1 g TMPTA in the presence of PI/Iod/EDB (0.3%/1%/1%, mol/mol/mol) was irradiated with a LED@405 nm under air in the mold. The generated polymer was immersed in 10 mL acetonitrile for 3 days. The amount of the extracted PI was determined using UV−visible spectroscopy.

2.8. 3D printing

A laser diode (Thorlabs, Exceter, United Kingdom) was used to obtain the specific 3D patterns on the basis of the photosensitive resins. The intensity of the laser on the sample surface was also about 110 $mW \cdot cm^{-2}$, and the spot size was around 50 μm. The direct laser write (DLW) experiment of the resin was carried out under air at room temperature. The obtained 3D patterns were analyzed by a numerical optical microscope (OLYMPUS DSX-HRSU).

3. Results and discussion

3.1. Synthesis of PIs

In this work, two different families of photoinitiators were examined. First, photoinitiators belonging to the family of the benzophenone-triphenylamines were prepared and obtained following a Friedel-Craft reaction between triphenylamine and benzoyl chloride. Thus, BT4 could be prepared by using two equivalents of benzoyl chloride, enabling to get the targeted molecule in 30% yield (see scheme 3). Similarly, BT1-BT3 were obtained with the same reaction, but by opposing triphenylamine to 4-methoxybenzoyl chloride.

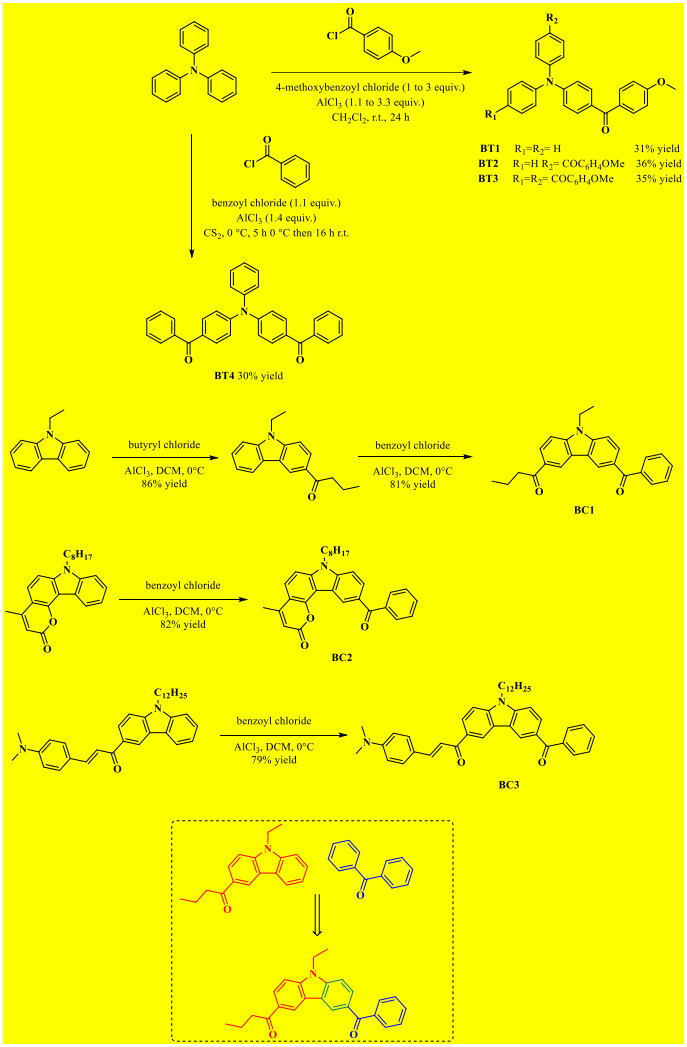

Scheme 3. Synthesis of the photoinitiator BT1-BT4, starting from triphenylamine and BC1-BC3 starting from various carbazole derivatives.

The number of equivalents of 4-methoxybenzoyl chloride were increased from 1 to 3 in order to give BT1, BT2, BT3 with reaction yields ranging from 31 to 36% (see scheme 3). Parallel to this, a second family of dyes was prepared, comprising carbazole as the main chromophore. Indeed, carbazole is extensively used for the design of visible-light photoinitiators and the combination with another well-known

photoinitiator i.e. benzophenone or coumarins can constitute another major advantage as synergetic effects can be expected between the two structures. An efficient strategy to access to these dual photoinitiators consist in fusing one aromatic ring of the two structures. By applying this strategy, BC1 was prepared in two steps, by mean of two successive Friedel-Craft reactions involving in first step butyryl chloride and in second step benzoyl chloride. A similar strategy was used for the synthesis of 10-benzoyl-4-methyl-7-octylpyrano[3,2-*c*]carbazol-2(7*H*)-one BC2 and 1-(6-benzoyl-9-dodecyl-9*H*-carbazol-3-yl)-3-(4-(dimethylamino)phenyl)prop-2-en-1-one BC3.

3.2. Light absorption properties

The UV-visible absorption spectra of the PIs in acetonitrile are shown in Figure 1 and the relevant parameters including their maximum absorption wavelengths (λ_{max}), their molar extinction coefficients at maximum absorption wavelength (ε_{max}) and their extinction coefficients at 405 nm (ε_{405nm}) are also presented in the Table 1. Compared to the BP and ITX, BT1-BT4 exhibit much better absorption properties visibly which can be ascribed to the benzophenone-triphenylamine hybrid structures. The maximum absorption wavelength of neat triphenylamine (TPA) is 300 nm and there is almost no absorption at 405 nm[27]. When the methoxybenzoyl substituents are introduced onto the TPA core, their absorption bands shift to the longer wavelengths. Meanwhile, extinction coefficients at maximum absorption wavelength increase obviously as the number of substituents on the TPA core increases from one to three for BT1, BT2 and BT3. Unsubstituted ethylcarbazole does not absorb the light nearly at above 370 nm, while BC1, BC2 and BC3 exhibit an absorption red-shifted at longer wavelength such as ε_{max}(BC3) = 409 nm. It can be ascribed to the strong π-conjugation extension effect. In addition, the PIs are characterized by high extinction coefficients at 405 nm (ε_{405nm}(BT2) = 5000 $M^{-1}cm^{-1}$, ε_{405nm}(BT3) = 6100 $M^{-1}cm^{-1}$, ε_{405nm}(BT4) = 6700 $M^{-1}cm^{-1}$, ε_{405nm}(BC3) = 26500 $M^{-1}cm^{-1}$) which can contribute to the photopolymerization using the light at 405 nm. The good light absorption properties of the different dyes ensure a good matching with the emission spectra of the near UV or the visible LEDs. Remarkably, all the proposed structures exhibit much better near-UV absorption than

the two benchmark PIs (BP and ITX) (See Figure 1).

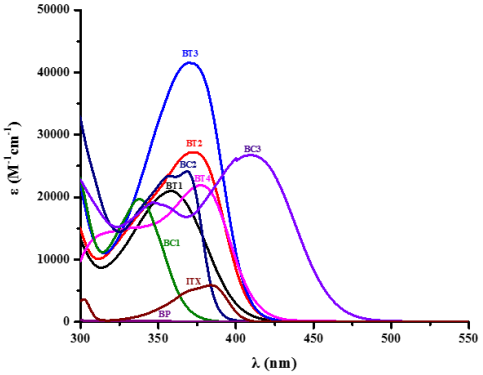

Figure 1. UV-visible absorption spectra of the different photoinitiators in acetonitrile.

Table 1. Light absorption properties of the different PIs.

PI	λ_{max} /nm	ε_{max} /$M^{-1}cm^{-1}$	ε_{405nm} /$M^{-1}cm^{-1}$
BT1	359	21000	1800
BT2	373	27200	5000
BT3	370	41600	6100
BT4	377	21700	6700
BC1	338	19700	20
BC2	369	24100	160
BC3	409	26700	26500
BP	340	160	0
ITX	383	5900	600

3.3. Free radical photopolymerization and cationic photopolymerization

Photopolymerization profiles of the acrylate functions of TMPTA in the presence of PI alone, PI/Iod, PI/EDB and PI/Iod/EDB systems are presented in Figure 2 and the final function conversions (FC) are summarized in Table 2. The polymerization was carried out under LED@405 nm irradiation in laminate. Because of the poor

polymerization profiles, BP-based PISs are not discussed in this study (almost no conversion with very poor polymerization profiles; See Figure 2, curves 9; final acrylate conversion < 10%).

Remarkably, without any additives, PI could initiate the polymerization of TMPTA alone (See Figure 2a). Remarkably, monocomponent Type II PI behavior was observed due to the H-abstraction of the benzophenone moiety from the monomer. BT2, BT3 and BT4-based systems showed higher final function conversions (FC = 51%, 56% and 49% respectively) than the ITX-based system (FC = 43%). It demonstrates that the H-abstraction abilities of BT2, BT3 and BT4 are stronger than that of ITX, and it is very significant for the Type II PI/amine systems.

In the presence of Iod, BT3 was the most efficient photoinitiator of the series, initiating the FRP of TMPTA through a photo-oxidation process in the presence of Iod as an additive (FC = 72%) (See Figure 2b). In addition, BT1, BT2, BT4, and BC3 also exhibited better performances than ITX, which is in agreement with their light absorption properties.

Interestingly, the two-component PI/EDB systems showed favorable performances (See Figure 2c). Because of the presence of the benzophenone moiety in the novel photoinitiator structures, conventional H-abstraction behavior (as well as photo-reduction process) in Type II system could be observed in the presence of EDB which play the role of H donor (as well as electron donor). Especially, BT3 displaying a trifunctional character exhibited excellent interaction ability with EDB so that the highest final function conversion (FC = 69%) for FRP of TMPTA could be obtained with this latter system. BT2/EDB and BT4/EDB also demonstrated higher final function conversions than the well-known ITX/EDB system during the FRP of TMPTA. While comparing to the BT3/EDB system, BT1/EDB and BC3/EDB systems showed lower polymerization rates during the FRP of TMPTA compared to the previous systems. It thus demonstrated that the photoinitiation ability is not only related to their absorption properties but also related to the number of benzophenone moieties in the chemical structures of photoinitiators. More reaction sites are provided for H-abstraction behavior from EDB in trifunctional benzophenone-triphenylamine hybrid

structures, which can promote the FRP more efficiently.

Three-component PI/Iod/EDB systems were also studied in the same conditions (See Figure 2d). BT1-BT4 and BC3-based systems showed better photoinitiation abilities than the benchmark ITX. The three-component BT3/Iod/EDB system could lead to the fastest polymerization rate and the highest final function conversion (77%), while the final function conversion initiated by ITX/Iod/EDB system was only of 61%.

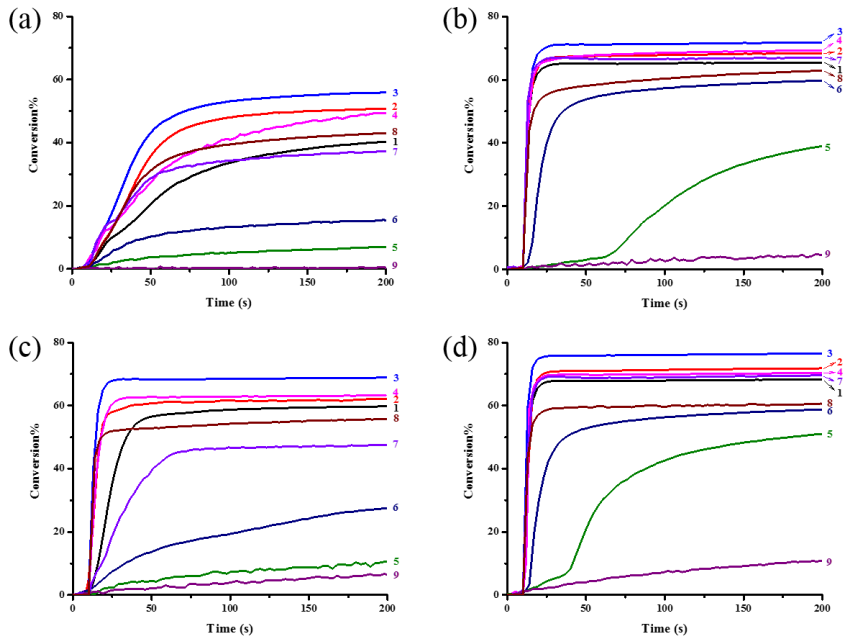

Figure 2. Photopolymerization profiles of TMPTA (acrylate function conversion vs. irradiation time) in laminate (~ 25 μm) under LED@405 nm irradiation in the presence of (a) PI alone (0.3%, mol), (b) PI/Iod (0.3%/1%, mol/mol), (c) PI/EDB (0.3%/1%, mol/mol), (d) PI/Iod/EDB (0.3%/1%/1%, mol/mol/mol): curve 1: PI = BT1; curve 2: PI = BT2; curve 3: PI = BT3; curve 4: PI = BT4; curve 5: PI = BC1; curve 6: PI = BC2; curve 7: PI = BC3; curve 8: PI = ITX; curve 9: PI = BP. The irradiation starts from t = 10 s.

The CP of epoxides was investigated in the presence of the different PI/Iod systems

upon irradiation with a LED@405 nm. Photopolymerization profiles of EPOX are depicted in Figure 3 and the final function conversions of epoxides are summarized in Table 2. Interestingly, good polymerization efficiency with both high final conversions and also good polymerization rates were obtained with several structures in thin samples under air. Notably, among all the investigated structures, BT3 possesses the highest molar extinction coefficient at 405 nm with regards to the other dyes and this compound is undoubtedly the most efficient photoinitiator examined in this work. The highest final epoxy function conversion FC = 47% was obtained at 200 s using BT3/Iod system. This behavior is directly related to the absorption properties of these compounds. Conversely, BC1 and BC2 based systems had low final epoxy function conversions (FC = 26% and FC = 27% respectively) due to unfavorable molar extinction coefficients at 405 nm. Even though a high extinction coefficient is observed at 405 nm (ε_{405nm}(BC3) = 26500 $M^{-1}cm^{-1}$), BC3 exhibited worse performances than ITX. It can be ascribed to the tertiary amine groups in BC3 structure which had a negative effect on the cation reactivity. Besides, the interaction of PIs with Iod and the kinds of cations could also be associated with the performance of CP.

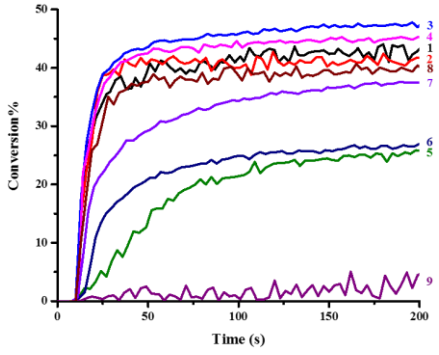

Figure 3. Photopolymerization profiles of EPOX (epoxy function conversion vs. irradiation time) under air (~ 25 µm) upon irradiation with the LED @405 nm in the presence of two-component systems PI/Iod (0.3%/1%, mol/mol): curve 1: PI = BT1; curve 2: PI = BT2; curve 3: PI = BT3; curve 4: PI = BT4; curve 5: PI = BC1; curve 6: PI = BC2; curve 7: PI = BC3; curve 8: PI = ITX; curve 9: PI = BP. The irradiation starts

from t = 10 s.

Table 2. Final acrylate function conversion for TMPTA and epoxy function conversion for EPOX under LED@405 nm irradiation at t = 200 s.

PISs	TMPTA/%				EPOX/%
	PI	PI/Iod	PI/EDB	PI/Iod/EDB	PI/Iod
BT1	40	65	60	68	43
BT2	51	68	62	72	41
BT3	56	72	69	77	47
BT4	49	69	63	70	45
BC1	7	39	11	51	26
BC2	15	60	28	58	27
BC3	37	67	48	70	38
ITX	43	58	56	61	40
BP	0	5	6	11	4

3.4. Photochemical reactivity

Steady state photolysis experiments were carried out to study the interaction activity of PIs with additives. BT3 which exhibited the best performance in photopolymerization was selected as the appropriate photoinitiator for the steady state photolysis experiments. As shown in Figure 4, UV-visible spectra of BT3-based systems in acetonitrile under LED@405 nm irradiation were recorded at different times. UV-visible absorption spectra of BT3 alone didn't change after 20 min of irradiation (See Figure 4a). In the presence of Iod, the maximum absorption wavelength of BT3 declined obviously after 60 s (Figure 4b) and the results indicated that there were effective interactions in the excited states between BT3 and Iod. Only a slight decrease of absorbance was observed for the BT3/EDB system (Figure 4c). It could be attributed to the H-abstraction reaction which occurred between the benzophenone moiety in BT3 and the tertiary amine moiety in EDB. Steady state photolysis experiments of BT3 in the presence of Iod and EDB were also performed in the same conditions (See Figure

4d). A distinct intensity decrement could be observed for the BT3/Iod/EDB three-component systems. Presence of isosbestic points during the kinetic showed that there was no by-side processes during the photoredox reaction of the BT3/Iod/EDB system. In addition, the consumption rate of BT3 in the BT3/Iod/EDB system seems to be slower than that of the BT3/Iod system. It is probable that there is a photoredox catalytic cycle in the three-component system which is discussed below.

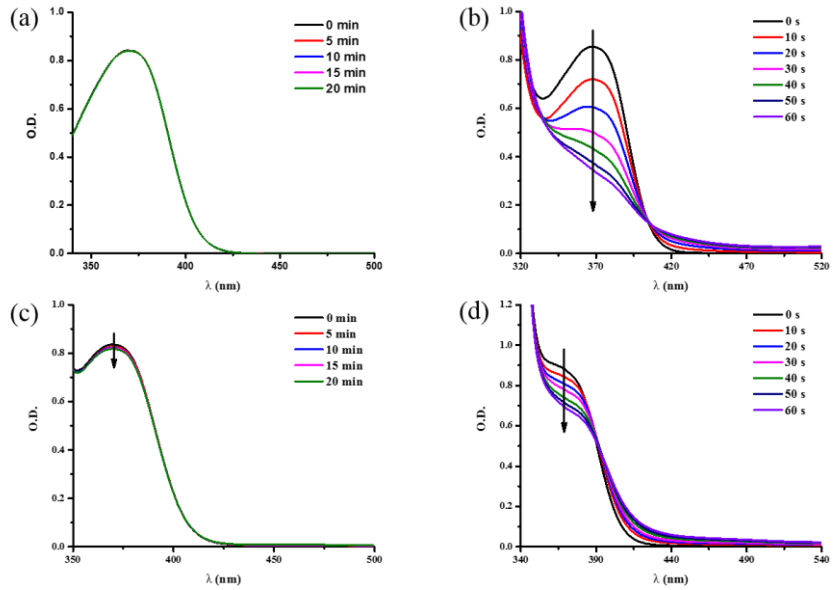

Figure 4. Photolysis of (a) BT3 alone; (b) BT3/Iod; (c) BT3/EDB; (d) BT3/Iod/EDB under LED@405 nm irradiation in acetonitrile ([Iod]=0.01M, [EDB]=0.01M).

Fluorescence quenching experiments are indicative of the interactions existing between the PIs and the different additives in the excited singlet states. The results obtained with the BT3/additives systems are shown in Figure 5 and the results obtained for the BT1, BT2, BT4 and BC3/additives systems are given in Figure S1-Figure S4. An efficient fluorescence quenching of BT3 by Iod and EDB was observed (See Figure 5a and Figure 5c) and high value of the Stern-Volmer coefficients (K_{sv}) were obtained (See Figure 5b and Figure 5d) (BT3/Iod interaction K_{sv} = 79 M^{-1}; BT3/EDB interaction

K_{sv} = 34 M^{-1}). In addition, the fluorescence lifetime (τ_0) of BT1, BT2 and BT3 in the absence of additives could be determined and the fluorescence decay profiles are given in Figure 6. Specifically, the fluorescence lifetimes of BT1, BT2 BT3 are 4.9 ns, 4.4 ns and 4.0 ns respectively. Therefore, the interaction rate constant of BT3/Iod and BT3/EDB are 19.6×10^9 $M^{-1}s^{-1}$ and 8.4×10^9 $M^{-1}s^{-1}$ which are almost diffusion controlled. And the higher interaction rate constant of BT3/Iod than that of BT3/EDB is also in agreement with the higher reactivity of the BT3/Iod system vs. BT3/EDB one. The parameters characterizing the reactivity of PIs with the additives are summarized in Table 3. The electron transfer quantum yields in the excited singlet state (Φ^{et}) for BT3/additives system are higher than those of BT1/additives and BT2/additives systems. Such as the electron transfer quantum yields $\Phi^{et}_{(EDB)}$ for BT1/EDB, BT2/ EDB, BT3/ EDB and BT4/ EDB systems are 0.46, 0.51, 0.56 and 0.52 respectively. It demonstrates that BT3 has a higher reactivity with EDB than BT1, BT2 and BT4 which is in full agreement with the results of photopolymerization. The electron transfer quantum yields $\Phi^{et}_{(EDB)}$ for BC3/EDB is 0.37 which indicates that the interaction between them is weak, so that the photopolymerization performance is unfavorable for the BC3/EDB system.

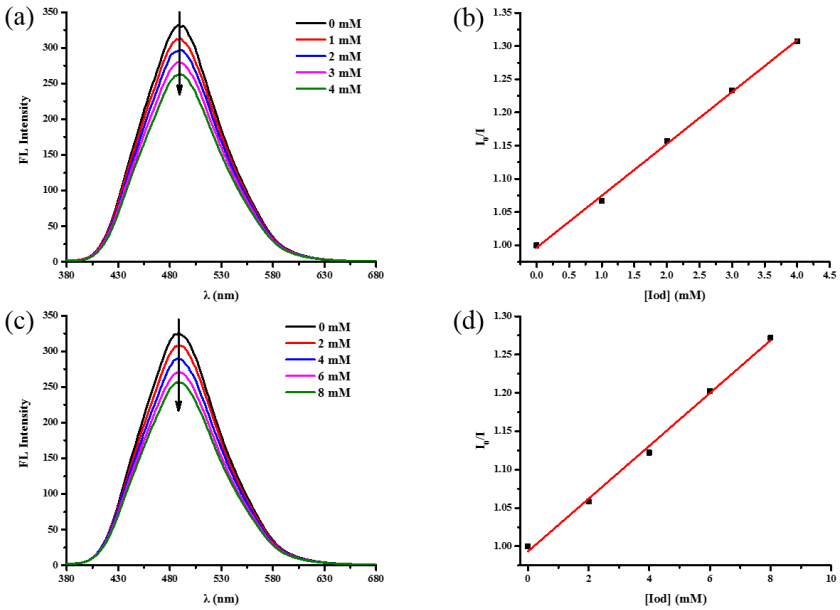

Figure 5. (a) Fluorescence quenching of BT3 by Iod in acetonitrile; (b) Stern–Volmer treatment for BT3/Iod fluorescence quenching; (c) Fluorescence quenching of BT3 by EDB in acetonitrile; (d) Stern–Volmer treatment for BT3/EDB fluorescence quenching.

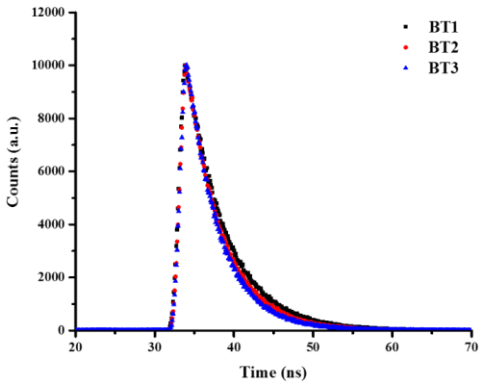

Figure 6. Fluorescence decay curves of BT1, BT2, BT3.

Table 3. Some parameters characterizing the reactivity of PIs with the additives.

PIs	$K_{SV(Iod)}$ /M^{-1}	$K_{SV(EDB)}$ /M^{-1}	$k_{q(Iod)}$ /$\times 10^9$ $M^{-1}s^{-1}$	$k_{q(EDB)}$ /$\times 10^9$ $M^{-1}s^{-1}$	τ_0 /ns	$\Phi^{et}_{(Iod)}$	$\Phi^{et}_{(EDB)}$
BT1	63	23	12.9	4.7	4.90	0.70	0.46
BT2	76	28	17.2	6.3	4.43	0.74	0.51
BT3	79	34	19.6	8.4	4.04	0.75	0.56
BT4	69	29	-	-	-	0.72	0.52
BC3	57	16	-	-	-	0.68	0.37

3.5. The free energy change (ΔG) of PIs and additives for electron transfer reactions in excited state.

The redox potentials of the PIs (E_{ox} and E_{red}) were obtained in acetonitrile by cyclic voltammetry. The crossing point of the absorption and fluorescence spectra allows the evaluation of the first singlet excited state energy levels (E_{S1}). Cyclic Voltammetry experiment and the singlet state energy determination of BT3 are depicted in Figure 7. The free energy changes (ΔG) in the excited singlet state for the electron transfer reaction between PIs (as electron donors) and Iod (as electron acceptor) could be calculated. Favorable free energy change (ΔG) were found (e.g. BT3/Iod: $\Delta G^{S1}_{Iod} = -0.96$ eV) and these results are in agreement with the strong PI/Iod interaction. In addition, the free energy changes (ΔG) for the electron transfer reaction between PIs (as electron acceptor) and EDB (as electron donors) were obtained (e.g. BT3/EDB: $\Delta G^{S1}_{EDB} = -0.88$ eV) which demonstrates that the electron transfer from EDB is feasible. Cyclic Voltammetry experiments and the singlet state energy determination of BT1, BT2, BT4 and BC3 are given in Figure S5 and Figure S6. All the parameters are summarized in Table 4.

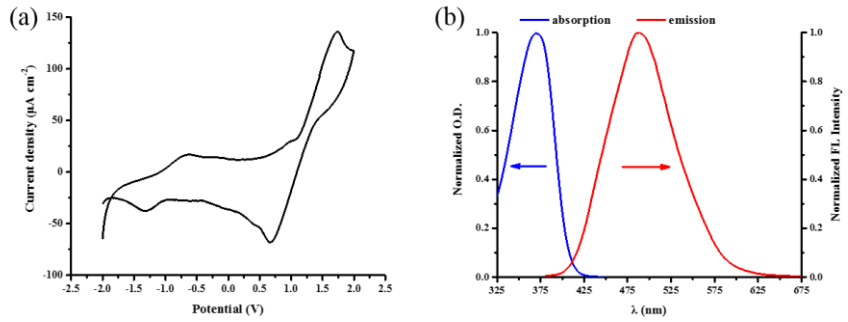

Figure 7. (a) Cyclic voltammograms of electrochemical reactions of BT3 in acetonitrile against saturated calomel electrode (SCE) under nitrogen saturated solution; (b) Singlet state energy determination of BT3.

Table 4. Redox potentials (E_{ox} and E_{red}) and singlet state energy (E_{S1}) for PIs; free energy changes (ΔG^{S1}) between PIs and additives in the excited singlet state.

PIs	E_{ox} /V	E_{red} /V	E_{S1} /eV	ΔG^{S1}_{Iod} /eV	ΔG^{S1}_{EDB} /eV
BT1	1.39	-0.35	2.92	-0.83	-1.57
BT2	1.07	-1.38	2.99	-1.22	-0.61
BT3	1.35	-1.13	3.01	-0.96	-0.88
BT4	0.94	-	3.00	-1.36	-
BC3	0.69	-1.42	2.64	-1.25	-0.22

3.6. Proposed photoinitiation mechanisms

Based on those results, the proposed photoinitiation mechanisms are presented in Scheme 4 (r1-r6) which demonstrates the formation of the reactive species used during the CP and the FRP. Under light irradiation, an electron of the photoinitiator is promoted from the ground state to the excited state ^{1,3}PI (r1). In photo-oxidation process, the electron transfer from PI to Iod generating aryl free radical Ar$^{\bullet}$ and cation BT$^{\bullet+}$ (r2) which are considered as the initiating species for the FRP and CP respectively.

In photo-reduction process, the interaction of PI and EDB underwent an electron

transfer and a H-abstraction to generate the radical $EDB_{(-H)}^{\bullet}$ which is the species responsible for the free radical polymerization (r3). This H-abstraction behavior was confirmed by ESR experiments. As shown in Figure 8, the hyperfine coupling constants of PBN radical adducts for BT3/EDB system are α_N = 14.4 G and α_H = 2.4 G, and it is in agreement with $EDB_{(-H)}^{\bullet}$ radical[29]. As a Type II photoinitiator, the interaction of BT3/EDB is depicted in r6. Compared to BT1 and BT2, the trifunctional character of BT3 provides more (consecutive) active sites for the H-abstraction reaction which accelerates the formation of $EDB_{(-H)}^{\bullet}$, so that a better polymerization performance is obtained in the presence of EDB.

Associated with the photolysis of BT3/Iod and BT3/Iod/EDB, the photoredox catalytic cycle was proposed in three-component BT3/Iod/EDB system (r4 and r5) which slows down the consumption of PI in photolysis. Meanwhile, the regeneration of BT3 speeds up the FRP.

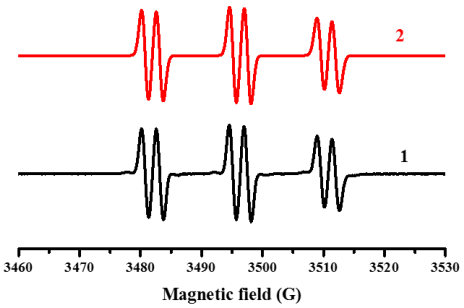

Figure 8. ESR-ST spectra of the radical adducts obtained in the presence of BT3/EDB under LED@405 nm irradiation in *tert*-butylbenzene (1) experimental spectrum; (2) simulated spectrum.

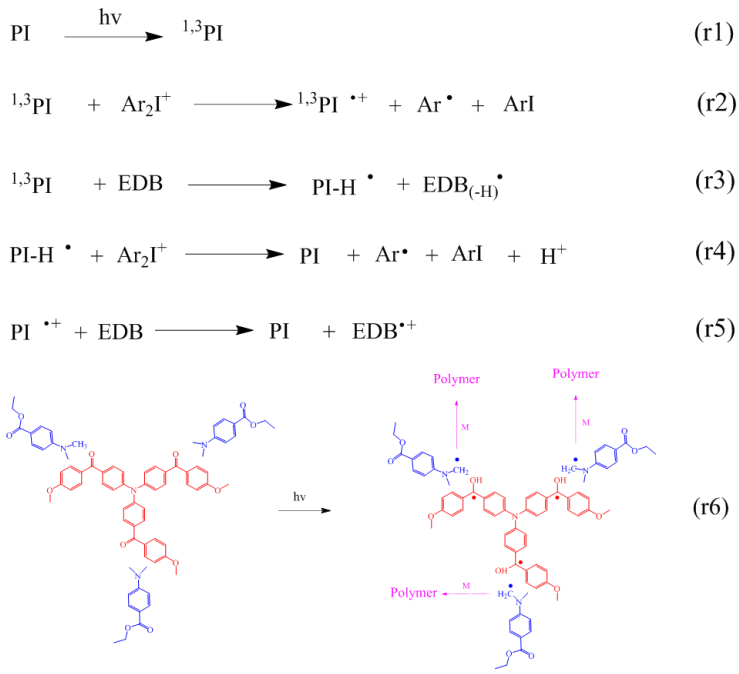

Scheme 4. Proposed photoinitiation mechanisms.

3.7. Migration study

The migration of PIs from the synthesized polymer using the PI/Iod/EDB (0.3%/1%/1%, mol/mol/mol) systems in TMPTA was evaluated in the UV-visible spectra. The generated polymer was immersed in acetonitrile for 3 days to extract the possible remaining photoinitiator. UV−visible absorption spectra of the solution obtained after the immersion of the polymer in acetonitrile are depicted in Figure 9 and the percentage of migration of PIs is shown in Table 5. The amounts of photoinitiators extracted in acetonitrile were 2.00%, 1.54%, 0.61% and 1.91% for the BT1-based system, BT2-based system, BT3-based system and ITX-based system respectively. As shown in r6 (see Scheme 4), in the presence of EDB, BT3 with the trifunctional character could generate more free radical BT3-H•. Through radical-radical self-couple, more dissociative BT3-H• could be fixed. Meanwhile, because of the high molecular weight of BT3 and the high crosslink density of the polymer network, only a slight amount of BT3 could be extracted. The favorable migration stability is helpful to reduce

the toxicity of the polymer and extend the application of PIs in more demanding areas.

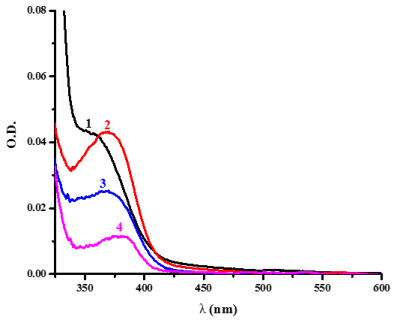

Figure 9. UV−visible absorption spectra of PIs extracted in acetonitrile from the polymer (1) BT1-based system, (2) BT2-based system, (3) BT3-based system, (4) ITX-based system.

Table 5. Migration of PIs in acetonitrile after 3 days of storage in acetonitrile.

PI	BT1	BT2	BT3	2-ITX
Migration /%	2.00	1.54	0.61	1.91

3.8. 3D printing

The three-component BT3/Iod/EDB system with the best performance for free radical photopolymerization of TMPTA was used for direct laser write (DLW) experiment. The experiment was carried with a computer-controlled laser diode at 405 nm and the sample was examined by numerical optical microscopy. As shown in Figure 10, the pattern “BT3” is up to 1650 μm and the high spatial resolution could be observed. Indeed, the high photosensitivity of BT3-based system allows a fast and effective polymerization process in the irradiated area.

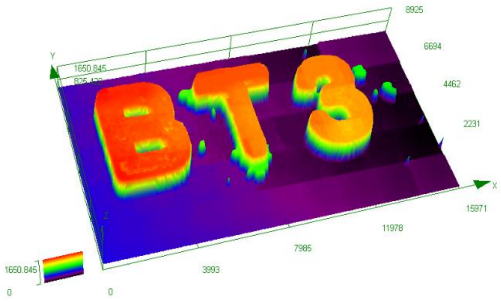

Figure 10. The 3D pattern is characterized by numerical optical microscopy.

3.9 Structure/reactivity/efficiency relationship

For benzophenone-triphenylamine PIs, the bifunctional and the trifunctional hybrid structures not only strengthened the light absorption properties but also provided more active sites for the H-abstraction reaction in the presence of EDB. As a result, BT2, BT3 and BT4 demonstrated better photoinitiation performances in FRP and CP than the monofunctional benzophenone-triphenylamine PIs BT1 and well-established ITX or BP. Because of the poor absorption properties, unfavorable polymerization behaviors were found for the benzophenone-carbazole PIs BC1 and BC2-based systems under LED@405 nm irradiation. Furthermore, there was a high extinction coefficient at 405 nm for BC3 and high acrylate function conversions were obtained in the presence of Iod. Weak interaction of BC3 and EDB was found which could be attributed to the amine groups in BC3 structure, so that BC3/EDB system had an unfavorable performance. In addition, the amine groups were also to the disadvantage of the cation species. So, low conversion of epoxy functions was found in the presence of BC3/Iod system.

4. Conclusion

In summary, four benzophenone-triphenylamine and three benzophenone-carbazole derivatives were developed as photoinitiators for photopolymerization under the LED irradiation. Six of the seven proposed structures have never been synthesized before. Because of the excellent absorption properties and reactivity, BT2, BT3 and

BT4 exhibited good performances in the presence of Iod in both FRP and CP. Interestingly, monocomponent Type II PI behavior was found and favorable performances were observed for these compounds in the presence of amine (EDB). The proposed mechanism was also investigated through the steady state photolysis, fluorescence and ESR-ST approaches. More interestingly, low migration property was found for BT3 due to the trifunctional character and high molecular weight. In addition, the BT3/Iod/EDB system was successfully applied on the 3D printing, and the 3D patterns showed high spatial resolution. The novel structures exhibit reasonable design route for the high-performance PIs and the development of other benzophenone-based PIs is under way.

Acknowledgments

The authors thank the China Scholarship Council (CSC No. 201906880009), the Aix Marseille University and The Centre National de la Recherche (CNRS) for financial supports. The Agence Nationale de la Recherche (ANR agency) is acknowledged for its financial support through the PhD grant of Guillaume Noirbent (ANR-17-CE08-0054) VISICAT project. The Direction Générale de l'Armement (DGA)/Agence Innovation Defense (AID) is acknowledged for its financial support through the PhD grant of Dr. Damien Brunel. PX acknowledges funding from the Australian Research Council (FT170100301).

References

(1) J. P. Fouassier; J. Lalevée. Photoinitiators for Polymer Synthesis. **2012**.

(2) Yagci, Y.; Jockusch, S.; Turro, N. J. Photoinitiated Polymerization: Advances, Challenges, and Opportunities. *Macromolecules* **2010**, *43*, 6245-6260.

(3) Dadashi-Silab, S.; Doran, S.; Yagci, Y. Photoinduced Electron Transfer Reactions for Macromolecular Syntheses. *Chemical Reviews* **2016**, *116*, 10212-10275.

(4) Shi, S.; Croutxé-Barghorn, C.; Allonas, X. Photoinitiating systems for cationic photopolymerization: Ongoing push toward long wavelengths and low light intensities. *Progress in Polymer Science* **2017**, *65*, 1-41.

(5) Aduba, D. C.; Margaretta, E. D.; Marnot, A. E. C.; Heifferon, K. V.; Surbey, W. R.; Chartrain, N. A.; Whittington, A. R.; Long, T. E.; Williams, C. B. Vat photopolymerization 3D printing of acid-cleavable PEG-methacrylate networks for biomaterial applications. *Materials Today Communications* **2019**, *19*, 204-211.

(6) del Barrio, J.; Sánchez-Somolinos, C. Light to Shape the Future: From Photolithography to 4D Printing. *Advanced Optical Materials* **2019**, *7*, 1900598.

(7) Li, F.; Song, Y.; Yao, M.; Nie, J.; He, Y. Design and properties of novel photothermal initiators for photoinduced thermal frontal polymerization. *Polymer Chemistry* **2020**, *11*, 3980-3986.

(8) Zivic, N.; Zhang, J.; Bardelang, D.; Dumur, F.; Xiao, P.; Jet, T.; Versace, D.-L.; Dietlin, C.; Morlet-Savary, F.; Graff, B.; Fouassier, J. P.; Gigmes, D.; Lalevée, J. Novel naphthalimide–amine based photoinitiators operating under violet and blue LEDs and usable for various polymerization reactions and synthesis of hydrogels. *Polymer Chemistry* **2016**, *7*, 418-429.

(9) Abdallah, M.; Le, H.; Hijazi, A.; Schmitt, M.; Graff, B.; Dumur, F.; Bui, T.-T.; Goubard, F.; Fouassier, J.-P.; Lalevée, J. Acridone derivatives as high performance visible light photoinitiators for cationic and radical photosensitive resins for 3D printing technology and for low migration photopolymer property. *Polymer* **2018**, *159*, 47-58.

(10) Tasdelen, M. A.; Lalevée, J.; Yagci, Y. Photoinduced free radical promoted cationic polymerization 40 years after its discovery. *Polymer Chemistry* **2020**, *11*, 1111-1121.

(11) Al Mousawi, A.; Dumur, F.; Garra, P.; Toufaily, J.; Hamieh, T.; Graff, B.; Gigmes, D.; Fouassier, J. P.; Lalevée, J. Carbazole Scaffold Based Photoinitiator/Photoredox Catalysts: Toward New High Performance Photoinitiating Systems and Application in LED Projector 3D Printing Resins. *Macromolecules* **2017**, *50*, 2747-2758.

(12) Schmitz, C.; Pang, Y.; Gülz, A.; Gläser, M.; Horst, J.; Jäger, M.; Strehmel, B. New High-Power LEDs Open Photochemistry for Near-Infrared-Sensitized Radical and Cationic Photopolymerization. *Angewandte Chemie International Edition* **2019**, *58*, 4400-4404.

(13) Fu, H.; Qiu, Y.; You, J.; Hao, T.; Fan, B.; Nie, J.; Wang, T. Photopolymerization of acrylate resin and ceramic suspensions with benzylidene ketones under blue/green LED. *Polymer* **2019**, *184*, 121841.

(14) Sun, K.; Pigot, C.; Chen, H.; Nechab, M.; Gigmes, D.; Morlet-Savary, F.; Graff, B.; Liu, S.; Xiao, P.; Dumur, F.; Lalevée, J. Free Radical Photopolymerization and 3D Printing Using Newly Developed Dyes: Indane-1,3-Dione and 1H-Cyclopentanaphthalene-1,3-Dione Derivatives as Photoinitiators in Three-Component Systems. *Catalysts* **2020**, *10*.

(15) Liu, S.; Brunel, D.; Sun, K.; Xu, Y.; Morlet-Savary, F.; Graff, B.; Xiao, P.; Dumur, F.; Lalevée, J. A monocomponent bifunctional benzophenone–carbazole type II photoinitiator for LED photoinitiating systems. *Polymer Chemistry* **2020**, *11*, 3551-3556.

(16) Xiao, P.; Zhang, J.; Dumur, F.; Tehfe, M. A.; Morlet-Savary, F.; Graff, B.; Gigmes, D.; Fouassier, J.

P.; Lalevée, J. Visible light sensitive photoinitiating systems: Recent progress in cationic and radical photopolymerization reactions under soft conditions. *Progress in Polymer Science* **2015**, *41*, 32-66.

(17) Pigot, C.; Noirbent, G.; Brunel, D.; Dumur, F. Recent advances on push–pull organic dyes as visible light photoinitiators of polymerization. *European Polymer Journal* **2020**, *133*, 109797.

(18) Dumur, F. Recent advances on pyrene-based photoinitiators of polymerization. *European Polymer Journal* **2020**, *126*, 109564.

(19) Chen, H.; Noirbent, G.; Sun, K.; Brunel, D.; Gigmes, D.; Morlet-Savary, F.; Zhang, Y.; Liu, S.; Xiao, P.; Dumur, F.; Lalevée, J. Photoinitiators derived from natural product scaffolds: monochalcones in three-component photoinitiating systems and their applications in 3D printing. *Polymer Chemistry* **2020**, *11*, 4647-4659.

(20) Liu, S.; Chen, H.; Zhang, Y.; Sun, K.; Xu, Y.; Morlet-Savary, F.; Graff, B.; Noirbent, G.; Pigot, C.; Brunel, D.; Nechab, M.; Gigmes, D.; Xiao, P.; Dumur, F.; Lalevée, J. Monocomponent Photoinitiators based on Benzophenone-Carbazole Structure for LED Photoinitiating Systems and Application on 3D Printing. *Polymers* **2020**, *12*.

(21) Dumur, F. Recent advances on carbazole-based photoinitiators of polymerization. *European Polymer Journal* **2020**, *125*, 109503.

(22) Tehfe, M.-A.; Dumur, F.; Graff, B.; Morlet-Savary, F.; Gigmes, D.; Fouassier, J.-P.; Lalevée, J. Design of new Type I and Type II photoinitiators possessing highly coupled pyrene–ketone moieties. *Polymer Chemistry* **2013**, *4*, 2313-2324.

(23) Zhou, T. F.; Ma, X. Y.; Han, W. X.; Guo, X. P.; Gu, R. Q.; Yu, L. J.; Li, J.; Zhao, Y. M.; Wang, T. D–D–A dyes with phenothiazine–carbazole/triphenylamine as double donors in photopolymerization under 455 nm and 532 nm laser beams. *Polymer Chemistry* **2016**, *7*, 5039-5049.

(24) Abdallah, M.; Dumur, F.; Graff, B.; Hijazi, A.; Lalevée, J. High performance dyes based on triphenylamine, cinnamaldehyde and indane-1,3-dione derivatives for blue light induced polymerization for 3D printing and photocomposites. *Dyes and Pigments* **2020**, *182*, 108580.

(25) Liu, S.; Brunel, D.; Sun, K.; Zhang, Y.; Chen, H.; Xiao, P.; Dumur, F.; Lalevée, J. Novel Photoinitiators Based on Benzophenone-Triphenylamine Hybrid Structure for LED Photopolymerization. *Macromolecular Rapid Communications* **2020**, https://doi.org/10.1002/marc.202000460.

(26) Sun, K.; Xu, Y.; Dumur, F.; Morlet-Savary, F.; Chen, H.; Dietlin, C.; Graff, B.; Lalevée, J.; Xiao, P. In silico rational design by molecular modeling of new ketones as photoinitiators in three-component photoinitiating systems: application in 3D printing. *Polymer Chemistry* **2020**, *11*, 2230-2242.

(27) Qu, J.; Kawasaki, R.; Shiotsuki, M.; Sanda, F.; Masuda, T. Synthesis and properties of polyacetylenes carrying N-phenylcarbazole and triphenylamine moieties. *Polymer* **2006**, *47*, 6551-6559.

(28) Tunc, D.; Yagci, Y. Thioxanthone-ethylcarbazole as a soluble visible light photoinitiator for free radical and free radical promoted cationic polymerizations. *Polymer Chemistry* **2011**, *2*, 2557-2563.

(29) Zhang, J.; Wang, S.; Lalevée, J.; Morlet-Savary, F.; Lam, E. S. H.; Graff, B.; Liu, J.; Xing, F.; Xiao, P. 1,2-Diketones as photoinitiators of both cationic and free-radical photopolymerization under UV (392 nm) or Blue (455 nm) LEDs. *Journal of Polymer Science* **2020**, *58*, 792-802.

Supporting Information

New Multifunctional Benzophenone-based Photoinitiators with High Migration Stability and the Application in 3D Printing

Shaohui Liu[1,2], Damien Brunel[3], Guillaume Noirbent[3], Alexandre Mau[1,2], Hong Chen[1,2], Fabrice Morlet-Savary[1,2], Didier Gigmes[3], Pu Xiao[4]*, Frédéric Dumur[3]*, Jacques Lalevée[1,2]*

[1]Université de Haute-Alsace, CNRS, IS2M UMR 7361, F-68100 Mulhouse, France
[2]Université de Strasbourg, France
[3]Aix Marseille Univ, CNRS, ICR UMR 7273, F-13397 Marseille, France
[4]Research School of Chemistry, Australian National University, Canberra, ACT 2601, Australia

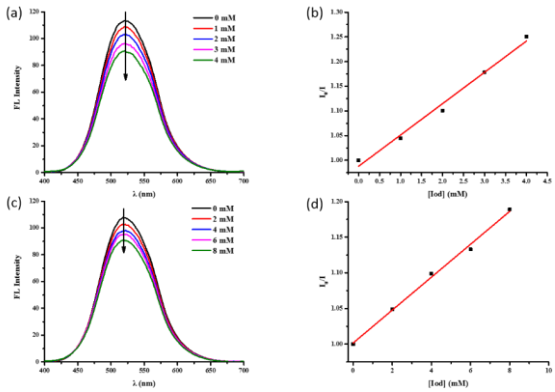

Figure S1. (a) Fluorescence quenching of BT1 by Iod in acetonitrile; (b) Stern–Volmer treatment for BT1/Iod fluorescence quenching; (c) Fluorescence quenching of BT1 by EDB in acetonitrile; (d) Stern–Volmer treatment for BT1/EDB fluorescence quenching.

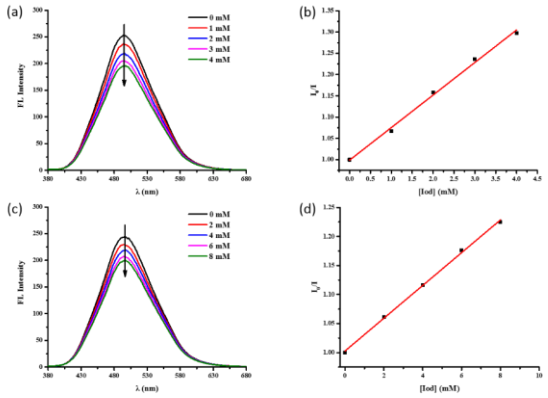

Figure S2. (a) Fluorescence quenching of BT2 by Iod in acetonitrile; (b) Stern–Volmer treatment for BT2/Iod fluorescence quenching; (c) Fluorescence quenching of BT2 by EDB in acetonitrile; (d) Stern–Volmer treatment for BT2/EDB fluorescence quenching.

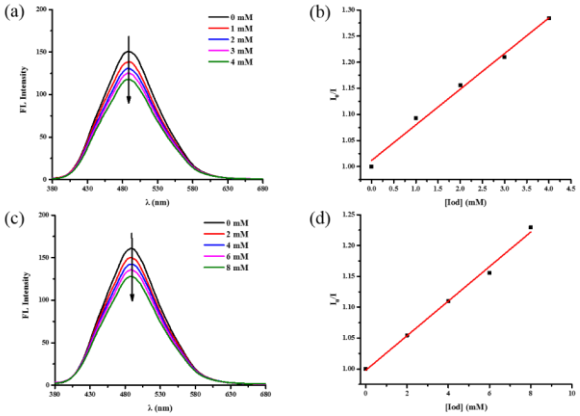

Figure S3. (a) Fluorescence quenching of BT4 by Iod in acetonitrile; (b) Stern–Volmer treatment for BT4/Iod fluorescence quenching; (c) Fluorescence quenching of BT4 by EDB in acetonitrile; (d) Stern–Volmer treatment for BT4/EDB fluorescence quenching.

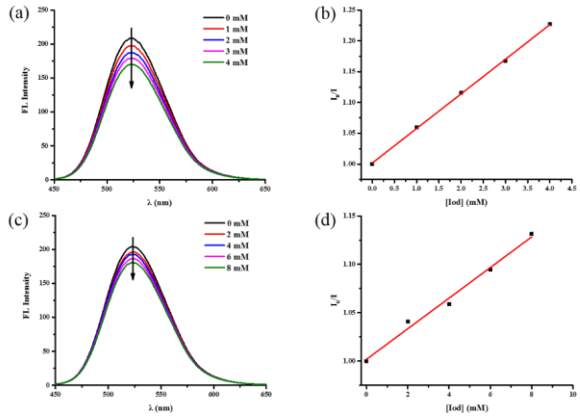

Figure S4. (a) Fluorescence quenching of BC3 by Iod in acetonitrile; (b) Stern–Volmer treatment for BC3/Iod fluorescence quenching; (c) Fluorescence quenching of BC3 by EDB in acetonitrile; (d) Stern–Volmer treatment for BC3/EDB fluorescence quenching.

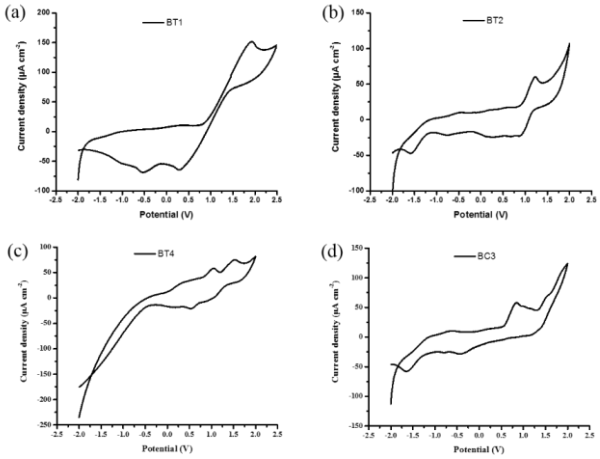

Figure S5. Cyclic voltammograms of electrochemical reactions of PIs in acetonitrile solvent against saturated calomel electrode (SCE) under nitrogen saturated solution: (a) BT1, (b) BT2, (c) BT4, (d) BC3.

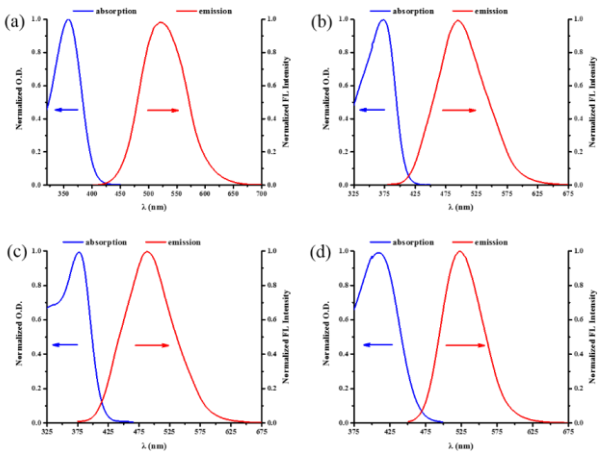

Figure S6. Singlet state energy determination in acetonitrile for: (a) BT1, (b) BT2, (c) BT4, (d) BC3.

Synthesis of (4-(diphenylamino)phenyl)(4-methoxyphenyl)methanone BT1

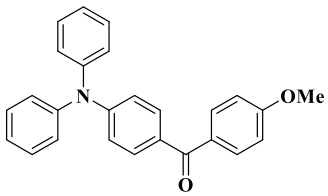

In a 100 mL one-necked round bottom flask were added triphenylamine (1.5 g, 6.11 mmol, 1 equiv., M= 245.33 g/mol) and aluminium chloride (0.9 g, 6.73 mmol, 1.1 equiv., M= 133.33 g/mol) in CH_2Cl_2 (40 mL). The reaction mixture was cooled to 0 °C and 4-methoxybenzoyl chloride (1.04 g, 6.11 mmol, 1 equiv., M= 170.9 g/mol) was added. The reaction mixture was stirred overnight. A large amount of cold water was added to quench the reaction and the reaction mixture was then extracted with CH_2Cl_2. The organic layer was washed with water and dried over $MgSO_4$. After filtration and solvent evaporation, a mixture of THF:pentane allow precipitation of the precipitate. The product (0.72 g, 31% yield) was obtained as white yellowish solid. ^1H NMR ($CDCl_3$) δ : 7.89 – 7.81 (m, 2H), 7.77 – 7.66 (m, 2H), 7.43 – 7.32 (m, 4H), 7.22 – 7.13

(m, 6H), 7.07 – 7.02 (m, 2H), 7.02 – 6.94 (m, 2H), 3.90 (s, 3H); ^{13}C NMR ($CDCl_3$) δ : 194.26, 162.86, 151.67, 146.83, 132.27, 131.78, 131.07, 130.54, 129.71, 125.98, 124.58, 120.02, 113.56, 55.58; HRMS (ESI MS) m/z: theor: 380.1645 found: 380.1649 ($[M+H]^+$ detected).

Synthesis of ((phenylazanediyl)bis(4,1-phenylene))bis((4-methoxyphenyl)methanone) BT2

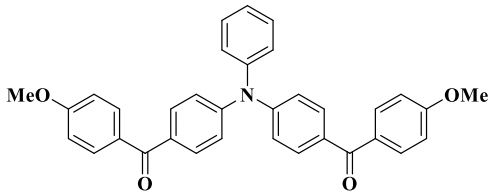

In a 100 mL one-necked round bottom flask were added triphenylamine (1.5 g, 6.11 mmol, 1 equiv., M= 245.33 g/mol) and aluminium chloride (1.79 g, 13.45 mmol, 2.2 equiv., M= 133.33 g/mol) in CH_2Cl_2 (40 mL). The reaction mixture was cooled to 0 °C and 4-methoxybenzoyl chloride (2.09 g, 12.23 mmol, 2 equiv., M= 170.59 g/mol) was added. The reaction mixture was stirred overnight. A large amount of cold water was added to quench the reaction and the reaction mixture was then extracted with CH_2Cl_2. The organic layer was washed with water and dried over magnesium sulfate. After filtration and solvent evaporation, THF and pentane allow formation of a solid. The product (1.14 g, 36% yield) was obtained as white yellowish solid. ^{1}H NMR ($CDCl_3$) δ : 8.09 (m, 4H), 7.98 – 7.92 (m, 4H), 7.60 – 7.58 (m, 2H), 7.46 – 7.44 (m, 3H), 7.33 – 7.28 (m, 4H), 7.25 – 7.21 (m, 4H), 4.16 (s, 6H); ^{13}C NMR ($CDCl_3$) δ : 194.18, 163.16, 150.46, 146.09, 133.62, 132.28, 131.65, 130.53, 130.27, 129.91, 129.59, 126.65, 125.85, 123.75, 122.31, 113.53, 55.52; HRMS (ESI MS) m/z: theor: 514.2013 found: 514.2013 ($[M+H]^+$ detected).

Synthesis of (nitrilotris(benzene-4,1-diyl))tris((4-methoxyphenyl)methanone) BT3

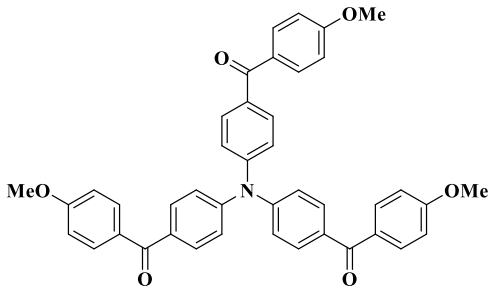

In a 100 mL one-necked round bottom flask were added triphenylamine (1.5 g, 6.11 mmol, 1 equiv., M= 245.32 g/mol) and aluminium chloride (2.69 g, 20.18 mmol, 3.3 equiv., M= 133.34 g/mol) in CH_2Cl_2 (40 mL). The reaction mixture was cooled to 0 °C and 4-methoxybenzoyl chloride (3.13 g, 18.34 mmol, 3 equiv., M= 170.59 g/mol) was added. The reaction mixture was stirred overnight. A large amount of cold water was added to quench the reaction and the reaction mixture was then extracted with CH_2Cl_2. The organic layer was washed with water and dried over magnesium sulfate. After filtration and solvent evaporation. A solid was formed and the product (1.4 g, 35% yield) was obtained as yellowish solid. ^{1}H NMR ($CDCl_3$) δ : 8.19 – 8.07 (m, 6H), 8.07 – 7.98 (m, 6H), 7.58 – 7.46 (m, 6H), 7.31 – 7.19 (m, 6H), 4.16 (s, 9H); ^{13}C NMR ($CDCl_3$) δ: 194.21, 163.24, 149.85, 133.71, 132.44, 131.84, 130.36, 123.84, 113.71, 55.63; HRMS (ESI MS) m/z: theor: 648.2381 found: 648.2376 ($[M+H]^+$ detected).

Synthesis of ((phenylazanediyl)*bis*(4,1-phenylene))*bis*(phenylmethanone) BT4

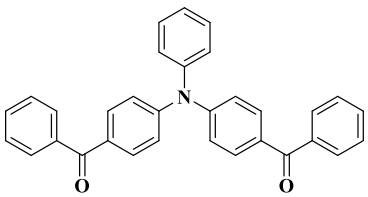

Triphenylamine (4.96 g, 20 mmol, 1 equiv., M= 145.33 g/mol) was added in a predried 100 mL two-necked round-bottom flask with a magnetic stirrer bar. Then aluminium chloride (3.8 g, 29 mmol, 1.4 equiv., M= 133.33 g/mol) was added to the round-bottom flask. The flask was evacuated under vacuum and flushed with nitrogen

for three times. 25 mL of carbon disulfide was added to the flask as the solvent and the mixture was stirred on an ice bath for several minutes. Benzoyl chloride (2.56 mL, 22 mmol, 1.1 equiv., M= 140.57 g/mol) was added dropwise to the reaction mixture on an ice bath. The mixture was stirred at 0°C for 5 hours. After solvent removal, 25 mL of deionized water was added to the reaction mixture. Suction filtration was applied to get crude product from reaction mixture and the crude product was washed with deionized water and absolute ethanol. The crude product was then redissolved in dichloromethane and was condensed. A column chromatography (SiO_2, hexane/chloroform/THF 30/8/1 as eluent) was used in order to obtain the product (2.79 g, 30% yield) as a yellowish solid. ^{1}H NMR ($CDCl_3$) δ : 8.15 – 8.13 (m, 2H), 8.12 – 8.10 (m, 2H), 7.83 – 7.73 (m, 4H), 7.66 – 7.56 (m, 3H), 7.52 – 7.44 (m, 6H), 7.25 – 7.06 (m, 6H); ^{13}C NMR ($CDCl_3$) δ : 195.44, 171.36, 133.88, 132.11, 130.35, 130.12, 129.91, 129.34, 128.64, 128.39, 126.97, 124.32, 122.42; HRMS (ESI MS) m/z: theor: 454.1802 found: 454.1805 ($[M+H]^+$ detected). Analyses were consistent with those reported in the literature [Y. Liu, X. Chen, Y. Lv, S.W.Y. Chen, J. Lam, F. Mahtab, H.S. Kwok, X. Tao, B.Z. Tang, Systemic Studies of Tetraphenylethene–Triphenylamine Oligomers and a Polymer: Achieving Both Efficient Solid-State Emissions and Hole-Transporting Capability. Chemistry – A European Journal 2012, 18, 9929–9938]

Synthesis of 1-(6-benzoyl-9-ethyl-9*H*-carbazol-3-yl)butan-1-one BC1

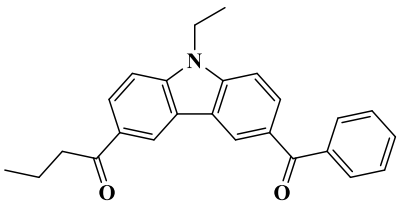

1-(9-Ethyl-9*H*-carbazol-3-yl)butan-1-one (0.45 g, 1.71 mmol, M = 265.36 g/mol) and benzoyl chloride (0.24 g, 0.20 mL, 1.71 mmol, d = 1.211, M = 140.57 g/mol) were dissolved in 10 mL DCM (stabilized with amylene) and the solution was cooled to 0°C. Then, $AlCl_3$ (0.43 g, 3.22 mmol, M = 133.33 g/mol) were added in one portion and the solution was stirred overnight. The reaction mixture was poured onto ice-water. The

solution was extracted several times with DCM. The organic phases were combined, dried over magnesium sulfate and the solvent removed under reduced pressure. The residue was filtered on a plug of silicagel using DCM as the eluent (0.51 g, 81% yield). ^{1}H NMR ($CDCl_3$) δ : 8.74 (d, *J* = 1.3 Hz, 1H), 8.64 (d, *J* = 1.2 Hz, 1H), 8.20 (dd, *J* = 8.7, 1.7 Hz, 1H), 8.10 (dd, *J* = 8.6, 1.7 Hz, 1H), 7.88 – 7.81 (m, 3H), 7.66 – 7.58 (m, 2H), 7.57 – 7.46 (m, 6H), 4.45 (q, *J* = 7.3 Hz, 2H), 3.08 (t, *J* = 7.3 Hz, 2H), 1.89 – 1.79 (m, 2H), 1.51 (t, *J* = 7.3 Hz, 3H), 1.05 (t, *J* = 7.4 Hz, 3H); ^{13}C NMR ($CDCl_3$) δ : 199.78, 196.41, 143.32, 143.22, 138.73, 138.66, 131.92, 131.89, 129.89, 129.69, 129.63, 129.56, 129.09, 128.99, 128.31, 126.90, 124.11, 124.07, 122.96, 122.86, 121.74, 108.73, 108.70, 108.67, 40.50, 38.18, 18.22, 14.01, 13.85; ; HRMS (ESI MS) m/z: theor: 370.1802 found: 370.1798 ($[M+H]^+$ detected).

Synthesis of 10-benzoyl-4-methyl-7-octylpyrano[3,2-*c*]carbazol-2(7*H*)-one BC2

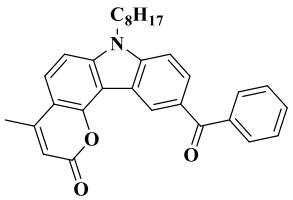

4-Methyl-7-octylpyrano[3,2-*c*]carbazol-2(7*H*)-one (0.62 g, 1.71 mmol, M = 361.48 g/mol) and benzoyl chloride (0.42 g, 0.35 mL, 3.00 mmol, d = 1.211, M = 140.57 g/mol) were dissolved in 10 mL DCM (stabilized with amylene) and the solution was cooled to 0°C. Then, $AlCl_3$ (0.43 g, 3.22 mmol, M = 133.33 g/mol) were added in one portion and the solution was stirred overnight. The reaction mixture was poured on ice-water. The solution was extracted several times with DCM. The organic phases were combined, dried over magnesium sulfate and the solvent removed under reduced pressure. The residue was filtered on a plug of silicagel using DCM as the eluent (0.65 g, 82% yield). ^{1}H NMR ($CDCl_3$) δ : 8.97 (d, *J* = 1.3 Hz, 1H), 8.04 (dd, *J* = 8.5, 1.3 Hz, 1H), 7.89 (d, *J* = 7.1 Hz, 2H), 7.62 (dd, *J* = 16.5, 8.0 Hz, 2H), 7.52 (t, *J* = 7.5 Hz, 2H), 7.47 (d, *J* = 8.6 Hz, 1H), 7.31 (d, *J* = 8.5 Hz, 1H), 6.16 (s, 1H), 4.35 (t, *J* = 7.0 Hz, 2H), 2.48 (s, 3H), 1.95 – 1.83 (m, 2H), 1.44 – 1.16 (m, 10H), 0.86 (t, *J* = 6.8 Hz, 3H); ^{13}C

NMR ($CDCl_3$) δ : 196.24, 160.65, 153.48, 150.14, 143.35, 142.38, 138.38, 132.15, 130.15, 130.11, 130.08, 128.39, 128.26, 126.56, 122.51, 120.50, 112.22, 111.29, 110.42, 108.57, 105.90, 43.73, 31.73, 29.27, 29.11, 29.02, 27.18, 22.57, 19.31, 14.04; HRMS (ESI MS) m/z: theor: 465.2304 found: 465.2307 ($M^{+\cdot}$ detected).

Synthesis of 1-(6-benzoyl-9-dodecyl-9*H*-carbazol-3-yl)-3-(4-(dimethylamino)phenyl) prop-2-en-1-one BC3

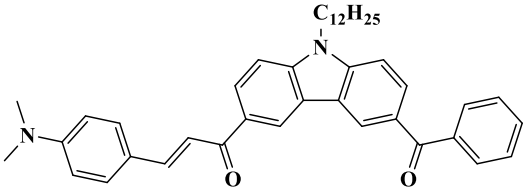

3-(4-(Dimethylamino)phenyl)-1-(9-dodecyl-9*H*-carbazol-3-yl)prop-2-en-1-one (4.35 g, 8.55 mmol, M = 508.75 g/mol) and benzoyl chloride (1.2 g, 1.0 mL, 8.55 mmol, d = 1.211, M = 140.57 g/mol) were dissolved in 50 mL DCM (stabilized with amylene) and the solution was cooled to 0°C. Then, $AlCl_3$ (2.15 g, 16.1 mmol, M = 133.33 g/mol) were added in one portion and the solution was stirred overnight. The reaction mixture was poured on ice-water. The solution was extracted several times with DCM. The organic phases were combined, dried over magnesium sulfate and the solvent removed under reduced pressure. The residue was filtered on a plug of silicagel using DCM as the eluent (4.14 g, 79% yield). ^{1}H NMR ($CDCl_3$) δ : 8.82 (d, *J* = 1.4 Hz, 1H), 8.68 (d, *J* = 1.4 Hz, 1H), 8.27 (dd, *J* = 8.7, 1.7 Hz, 1H), 8.09 (dd, *J* = 8.6, 1.7 Hz, 1H), 7.90 – 7.85 (m, 3H), 7.64 – 7.52 (m, 6H), 7.49 (d, *J* = 8.6 Hz, 2H), 6.72 (d, *J* = 8.9 Hz, 2H), 4.37 (t, *J* = 7.2 Hz, 2H), 3.04 (s, *J* = 8.6 Hz, 6H), 1.98 – 1.86 (m, 2H), 1.43 – 1.23 (m, 18H), 0.87 (t, *J* = 6.9 Hz, 3H); ^{13}C NMR ($CDCl_3$) δ : 196.60, 189.60, 152.06, 145.18, 143.82, 143.73, 138.90, 131.99, 131.50, 130.50, 130.04, 129.53, 128.99, 128.43, 127.45, 124.28, 123.10, 123.01, 122.93, 121.97, 117.03, 112.01, 109.17, 109.04, 43.76, 40.26, 32.01, 29.70, 29.65, 29.57, 29.46, 29.43, 29.09, 27.35, 22.79, 14.22. HRMS (ESI MS) m/z: theor: 613.3789 found: 613.3787 ($[M+H]^+$ detected).

^{1}H NMR of 1-(6-benzoyl-9-ethyl-9*H*-carbazol-3-yl)butan-1-one BC1

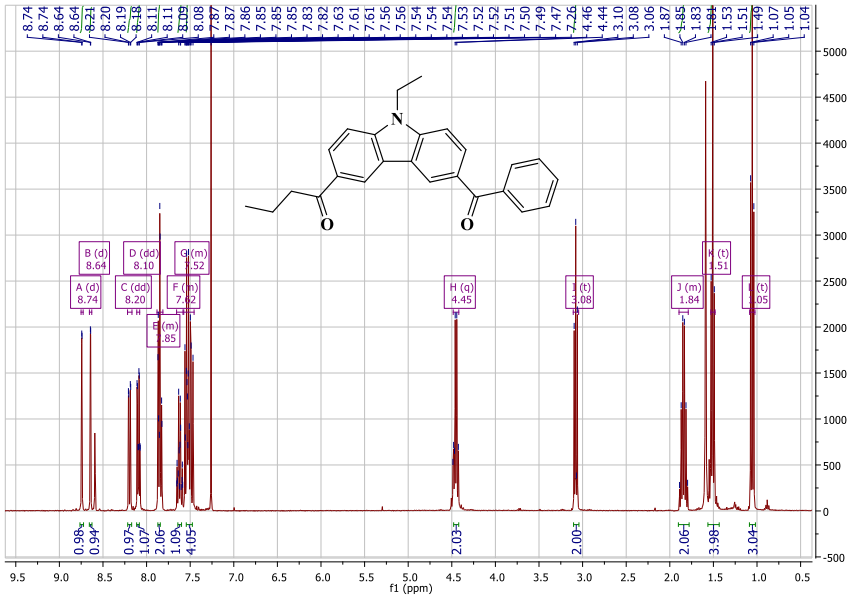

^{13}C NMR of 1-(6-benzoyl-9-ethyl-9*H*-carbazol-3-yl)butan-1-one BC1